HT-FED2004-56325

LARGE EDDY SIMULATION OF THE FLOW AROUND AN AHMED BODY

Siniša Krajnović [*]
Department of Thermo and Fluid Dynamics
Chalmers University of Technology
SE-412 96 Göteborg
Sweden
Email: sinisa@tfd.chalmers.se

Lars Davidson
Department of Thermo and Fluid Dynamics
Chalmers University of Technology
SE-412 96 Göteborg
Sweden
Email: lada@tfd.chalmers.se

ABSTRACT

A new approach for large eddy simulation (LES) of the flows around ground vehicles is demonstrated. It is based on the character of the flow with large regions of recirculations rather than on traditional resolution requirements for the LES of wall bounded flows. Recommendations for preparing and realization of LES for vehicle flows are presented and validated on a test case of the flow around an Ahmed body with the 25° angle of the rear slanted surface. Comparison of the LES results with the experimental data proved the validity of this new method.

INTRODUCTION

It has been known for a long time that the shape of a ground vehicles determines their aerodynamic properties. A modification of the shape that produces better aerodynamic properties requires thorough understanding of the turbulent flow around vehicles. Unfortunately, today after several decades of experimental and numerical studies, our understanding of the flow around ground vehicles is often limited to qualitative picture of the time-averaged large flow structures. Experimental techniques were first to be adopted in the studies of flows around ground vehicles and they are still more used than numerical methods in the design. Although the numerical simulations have been conducted in the automobile companies, they have failed to predict the flows observed in the experimental observations. Only recently the numerical simulations have taken over the role of some experimental studies and become design tool in some of the automobile companies (such as Volvo Cars). Both experimental and numerical methods have their advantages and disadvantages. Measuring techniques are limited to a part of the domain and are often used to measure time-averaged flow rather than temporal development of the instantaneous flow. The computational fluid dynamics (CFD) can easily provide the spatial information about the flow in the entire domain (virtual wind tunnel). Before we discuss the ability of CFD to predict development of the flow in time (i.e. temporal information), it is appropriate to make some remarks about the CFD results.

Turbulent scales in the flow around ground vehicle range from those of the size of the vehicle to microscopic ones. Unfortunately most turbulent scales in this flow are small owing to high Reynolds number making resolution requirements very high. This makes the solution of time-dependent Navier-Stokes equations for the flows around ground vehicles at operating velocities infeasible. As a result of the limitations of the computer resources, simulations of time-averaged (RANS) equations have mostly been used in the literature.

Instead of using real vehicles, very simplified (generic) vehicle models are often used to study how flow changes with geometry. Using such an approach we can isolate few geometric properties and study their influence on the flow.

The pioneering work by Ahmed *et al* (1984) had the objective to study the influence of the angle between the roof and the rear end slanted surface of a car with a typical fastback geometry (such as Volkswagen Golf I or Volkswagen Polo I). Their investigation showed a clear influence of the rear slant angle to the time-averaged flow structures. As they varied this angle they found

---

[*]Address all correspondence to this author.

1

that the flow changes the character at the angle of about 30°. Such a strange behavior of the flow with very simple change in the geometry attracted researchers to perform further experimental and numerical studies of this flow. Some of the experimental studies are described by Spohn and Gillieron (2002) and Lienhart and Becker (2003). Numerical studies such as those made by Han (1989) and described in Manceau and Bonnet (2000) are used to validate the CFD technique (often RANS simulation). Large number of RANS simulations (using different turbulence models) and one large eddy simulation (LES) of the flow around body defined by Ahmed *et al* (1984) are presented by Manceau and Bonnet (2000). Only two angles of the rear slanted surface, 25° and 35°, were considered in these simulations. The results of these simulations were compared with the experimental data produced by Lienhart and Becker (2003). The main conclusion from these simulations was that while the simulations were relatively successful in prediction of the 35° case, they were unsuccessful in the 25° case.

The aim of this paper is to demonstrate that if carefully applied, the LES can give accurate representation of the flow with the rear slant angle of 25° case. As we already mentioned, the LES of this flow was already presented (Manceau and Bonnet (2000)) and showed poor agreement with the experimental observations. This failure of LES presented in this reference shows either that LES is unable to predict this flow or that it requires different approach from that in Manceau and Bonnet (2000) and very careful preparation and realization.

GENERIC GROUND VEHICLE BODY

The generic vehicle body was chosen to be the same as used in the experiments by Ahmed *et al* (1984) and Lienhart and Becker (2003). The geometry of the body and the computational domain are given in Fig. 1. All the geometric quantities are normalized with the body height, H, equal to 0.288 m. The values of the geometric quantities are $L/H = 3.625$, $l_r/H = 2.928$, $G/H = 0.697$, $W/H = 1.35$ and $S/H = 2.571$. The front part is rounded with a radius of $R/H = 0.347$ in the symmetry planes $y = 0$ and $z = 0$. The geometry of the rounded corners was made from the data (in form of distinct points) measured at the body used in Ahmed *et al* (1984) and Lienhart and Becker (2003). The flow with the rear body slant angle $\alpha = 25^o$ is considered in this paper since it was found difficult to predict in previous RANS and LES simulations (Manceau and Bonnet (2000)). This body is placed in the channel with cross section of $B \times F = 6.493H \times 4.861H$ (width $\times$ height). The cross section of this channel is identical with the open test section of the wind tunnel used in the experiments of Lienhart and Becker (2003). The front face of the body is located at the distance of $x_1 = 7.3H$ from the channel inlet and the downstream length between the rear face of the body and the channel outlet is $x_2 = 21H$. The body is lifted from the floor producing the ground clearance of

$c/H = 0.174$, same as in the experiments. The Reynolds number, based on the incoming velocity U_∞ and the car height H, of $Re = 7.68 \times 10^5$ used in the experiments Lienhart and Becker (2003) was reduced to $Re = 2 \times 10^5$. Krajnović and Davidson (2003) have already demonstrated successful LES of this lower Reynolds number case with no rear body slant angle, i.e. $\alpha = 0^o$ (generic bus body). We expect that the slanted rear end will produce a wider spectrum of turbulent scales that must be resolved in LES.

MAKING LARGE EDDY SIMULATION

Resolution requirements of the near-wall regions in attached flows such as channel flow or a flat plate flow are similar to those in direct numerical simulations. This is because the coherent structures (so called low- and high-speed streaks) near the walls are responsible for the most of the turbulence production in the boundary layer. Thus an accurate representation of these structures is crucial for the result of the LES of the flat plate flow for example.

Flows around bluff bodies such as that around ground vehicles are different from the channel or the flat plate flows. They contain a number of separating regions with large coherent structures that contain much more turbulent energy than the near-wall structures. Let us consider the following question. What is the size of the smallest turbulent structures that must be resolved in a LES of the flow around ground vehicles?

In the regions of the separated flow (such as the wake behind the vehicle) the transport of momentum is dominated by large recirculating motions of the flow and the influence of the small near wall structures is limited. Thus the structures that must be resolved in this region are the smallest "large" (recirculating) structures. What about the attached regions in the flow around the vehicle? The answer to this question is dependent on what part of the flow is our main interest. Prediction of drag is often the main objective of the CFD study in vehicle aerodynamics. As the pressure drag is much larger than the friction drag and is dominated by the low pressure in the wake, prediction of the wake flow is crucial. Does this mean that it is sufficient to predict the wake flow and ignore the resolution requirements for the regions located upstream from the wake? The wake flow is influenced by the upstream flow, but the question is how strong this influence is. The boundary layer developed on the roof surface of the body separates at the location where the roof goes over to the rear face of the body. We can distinct between two main situations. First, the changeover from the roof to the rear face can be continuous such as that in the circular cylinder. In that case the position of the separation and the nature of the downstream flow is determined by the upstream history of the flow. The second situation is when the geometry defines the separation of the flow such as in the generic car body studied in this paper. How big is the influence of the upstream flow on the wake in this case? Is

2

the resolution of the upstream boundary layer equally important here as in the case with the continuous changeover in the surface geometry? We believe that in this case the influence of the geometry is much larger than that of the upstream history of the flow.

OUR APPROACH

Although we assume that in the flow around our generic body, the upstream boundary layer has limited influence on the flow in the wake, we cannot neglect it. Thus we should try to predict the near wall region as good as possible. Unfortunately the near wall coherent structures decrease in size with the Reynolds number and for the Reynolds number used in the experiments by Lienhart and Becker (2003), the task of resolving these structures is overwhelming (see Krajnović (2002) for the estimate of the computational cost for the resolution of the near-wall structures in the flow around ground vehicle body).

We have already assumed that the geometry rather than the upstream flow defines the flow in the wake. Here we make another assumption. *The magnitude of the Reynolds number is less important for the recirculating flow in the wake than for the boundary layer.* Together with the dependence of the wake flow on the geometry this means that we can reduce the Reynolds number in our LES and obtain a flow similar to that in the experiment that is characterized by the higher Reynolds number. We emphasize that these are still only *hypothesis*.

If our hypothesis of Reynolds number independence of the wake flow is correct, how much can we lower the Reynolds number and still obtain this independence? This is not clear but the simulated flow on the roof should be as similar as possible to that in the experiment at high Reynolds number. Thus if the high Reynolds number roof flow does not separate at the leading edge, our simulated low Reynolds number flow should not separate or should have as small separated regions as possible. Our knowledge about the dependence of the Reynolds number and the shape of the front of the ground vehicle (i.e. roundedness of the leading edges) is poor and is limited to the dependence of the drag coefficient on the Reynolds number and the roundedness of the leading edges of the prismatic bodies (Cooper (1985)). As the information about the flow on the roof, lateral sides and the under-body is not available from the experiments, we don't know if the flow separates on these surfaces. However, we can draw some conclusions from our previous LES of the flow around a similar body (Krajnović and Davidson (2003)). As the front of the body is more rounded and the Reynolds number is higher in Lienhart and Becker (2003) (body studied in this paper) than in Krajnović and Davidson (2003) we conclude that the separated regions, if they exist, are smaller around the front of the body here than on the body in Krajnović and Davidson (2003). Krajnović and Davidson (2003) showed that LES can predict the flow around the ground vehicle body that is character-

ized with Reynolds number of about 2×10^5 (based on the hight of the body and the velocity at the inlet). Thus we choose for our LES the Reynolds number of 2×10^5 instead of the experimental 7.68×10^5 (thus about four times lower LES Reynolds number compared to the experimental one).

PREPARATION AND REALIZATION OF LES

Most LES of the flow around bluff bodies are using structured hexahedral meshes which give better accuracy than for example tetrahedral meshes. Making a structured hexahedral mesh so that the computational cells are concentrated where they are needed is far from trivial even around relatively simple bluff body such as the ground vehicle body studied in this paper. Providing the optimal structured mesh for the detailed passenger car would be quite a challenge.

Here we shall demonstrate one of the approaches that can be used to concentrate most of the cells in the region around the body. Instead of using only H grid topology that spread the fine resolution in the boundary layer of the body all the way to the boundaries of the wind tunnel, we use a combination of O and C grid topologies (see Fig. 2) that makes local refinement of the grid possible. The topology of the grid consists of an O grid, with a thickness of $0.1H$ and a C grid around the O grid (see Fig. 2). An additional 'dummy' car surface was made around the real car and the O grid was projected on these two surfaces. The rest of the blocking structures was made using H grids. This strategy resulted in the following distribution of the computational cells. The O grid (i.e. the region in a belt of thickness $0.1H$ around the body) contained 4.4 and 7.5 million cells of totally 9.6 and 16.5 million cells in the medium and the fine grids, respectively. The region containing the O and the C grids together (i.e. the region in a belt of thickness $0.28H$ around a car) hold 6.3 and 10.8 million cells in the medium and the fine grids, respectively.

Unlike the results of steady RANS simulations, the results of time-dependent LES are dependent on the time where we start to monitor our results (i.e. when the fully developed flow is obtained). Unfortunately, in the LES of the flow around ground vehicles the fully developed flow is unknown and must be computed. The initial fully developed flow is often computed from the fluid at rest (as in this paper) or from a previous solution of RANS simulation. How do we know that the flow has become fully developed? Probably, the only way to be sure that the flow has developed is the 'a posteriori' one (i.e. after the entire simulation). Such a test could prove that the mean, RMS values and the spectral picture of the solution are not dependent on the position in time where we started sampling of the solution. As we need to start the time averaging before we can perform the 'a posteriori' test, some approximate method must be used to ensure that the characteristics of the flow are not changing. We monitored the time required for the fluid particle to travel from the front to the rear face of the car body. We then computed the
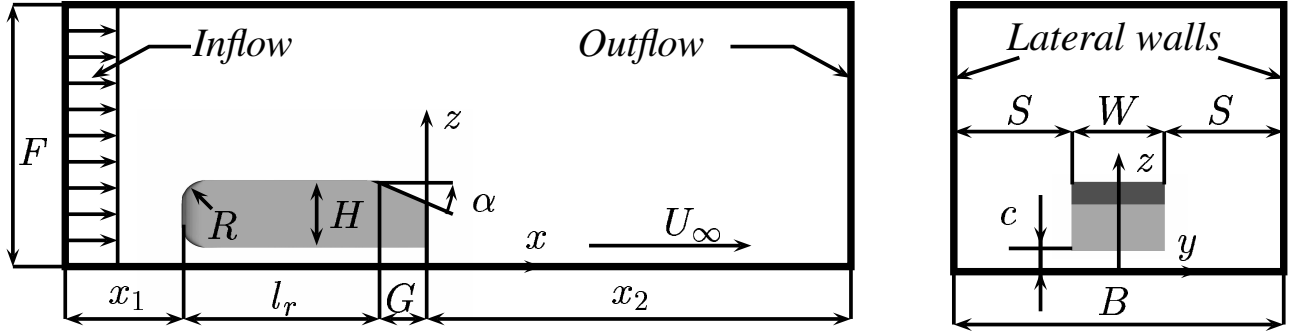
3

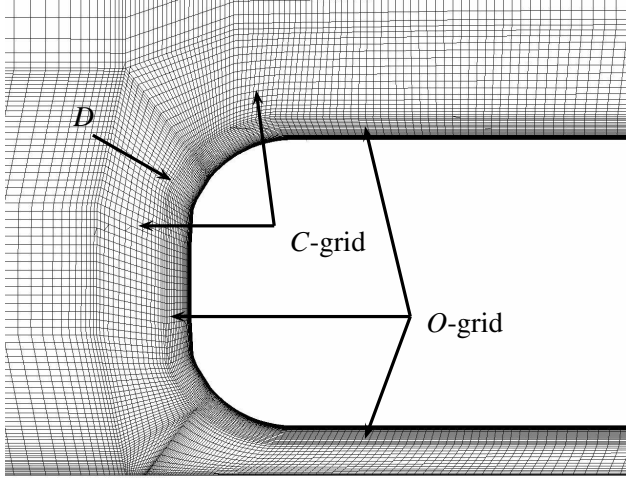Figure 1. Schematic representation of the computational domain with vehicle body.

Figure 2. The computational mesh in symmetry plane $y = 0$. D indicates the position of the dummy surface. View from the lateral side.

mean and the RMS values of the global quantities (aerodynamic forces) and local variables (velocity components and pressure in several points in and around the wake behind the body) for this time interval. The Fourier transforms of both global and local quantities were computed but because of the relatively short time sequences we could rely only on the high frequency events. The time averaging was started when there were no significant differences in the mean and the instantaneous information between two sequential time sequences. Computational cost for obtaining the fully developed flow is significant and for the simulations presented in this paper the computational time for obtaining fully developed conditions were roughly one fourth of the total time of the simulations.

When the flow has evolved to become fully developed, monitoring of the instantaneous results and their averaging can begin. Numerical time steps in LES are short to retain accuracy. The short time steps lead to large number of time steps for resolving the low frequency events and the time averaging. Our experi-

ence is that the number of time steps required for resolving the low frequency events is larger than that needed for obtaining of the time-averaged results (see Krajnović and Davidson (2003)). Thus in this work we shall confine our simulation to provide time-averaged results that are not a functions of time (i.e. the averaging time is long enough) rather than resolve all low frequency turbulence events. The symmetry of the flow around the symmetry plane ($y = 0$ plane) was used in this paper as a proof of long enough averaging time.

GOVERNING EQUATIONS AND SUBGRID-SCALE MODELING

The governing LES equations are the incompressible Navier-Stokes and the continuity equations filtered with the implicit spatial filter of characteristic width Δ (Δ is the grid resolution in this work):

$$\frac{\partial \bar{u}_i}{\partial t} + \frac{\partial}{\partial x_j}(\bar{u}_i \bar{u}_j) = -\frac{1}{\rho}\frac{\partial \bar{p}}{\partial x_i} + \nu \frac{\partial^2 \bar{u}_i}{\partial x_j \partial x_j} - \frac{\partial \tau_{ij}}{\partial x_j} \qquad (1)$$

and

$$\frac{\partial \bar{u}_i}{\partial x_i} = 0. \qquad (2)$$

Here, $\bar{u}_i$ and $\bar{p}_i$ are the resolved velocity and pressure, respectively, and the bar over the variable denotes filtering.

These equations are derived applying a filtering operation

$$\bar{f}(x_i) = \int_\Omega f(x_i')G(x_i, x_i')dx_i' \qquad (3)$$

on the Navier-Stokes and the continuity equations. Here G is a top hat filter function and Ω represents the entire flow domain. The filtered variables in the governing Eqs. (1) and (2) are obtained implicitly through the spatial discretization.

The goal of the filtering is to decompose the fluid motion into a large-scale component that are resolved and the small subgrid scale (SGS) that are modeled. The influence of the small scales of the turbulence on the large energy carrying scales in Eq. (1) appears in the SGS stress tensor, $\tau_{ij} = \overline{u_i u_j} - \bar{u}_i \bar{u}_j$. The algebraic eddy viscosity model originally proposed by Smagorinsky (1963) is used in this paper for its simplicity and low computational cost. The Smagorinsky model represents the anisotropic part of the SGS stress tensor, τ_{ij}, as:

$$\tau_{ij} - \frac{1}{3}\delta_{ij}\tau_{kk} = -2\nu_{sgs}\bar{S}_{ij} \tag{4}$$

where $\nu_{sgs} = (C_s f \Delta)^2 |\bar{S}|$ is the SGS viscosity,

$$\bar{S}_{ij} = \frac{1}{2}\left(\frac{\partial \bar{u}_i}{\partial x_j} + \frac{\partial \bar{u}_j}{\partial x_i}\right) \tag{5}$$

is the resolved rate-of-strain tensor and $|\bar{S}| = \left(2\bar{S}_{ij}\bar{S}_{ij}\right)^{\frac{1}{2}}$. f in the expression for the SGS viscosity is the van Driest damping function

$$f = 1 - exp\left(\frac{y^+}{25}\right) \tag{6}$$

Using this damping function, wall effects are partially taken into account by 'damping' the length scale $l = C_s f \Delta$ near to the walls. The value of $C_s = 0.1$ previously used for bluff-body flows (Krajnović and Davidson (2002)) and flow around simplified bus (Krajnović (2002), Krajnović and Davidson (2003)) is used in this work. The filter width, Δ, is defined in this work as $\Delta = (\Delta_1 \Delta_2 \Delta_3)^{1/3}$, where Δ_i are the computational cell sizes in three coordinate directions.

BOUNDARY CONDITIONS AND NUMERICAL DETAILS

The average turbulent intensity at the inlet of the wind tunnel used in the experiments of Lienhart and Becker (2003) was 0.25%. A uniform velocity profile constant in time was thus used as the inlet boundary condition in our LES. The convective boundary condition $\partial \bar{u}_i / \partial t + U_c (\partial \bar{u}_i / \partial x) = 0$ was used at the downstream boundary. Here, U_c was set equal to the incoming mean velocity, U_∞. The lateral surfaces and the ceiling were treated as slip surfaces using symmetry conditions ($\partial \bar{u}/\partial z = \partial \bar{w}/\partial z = \bar{v} = 0$ for the lateral sides and $\partial \bar{u}/\partial z = \partial \bar{v}/\partial z = \bar{w} = 0$ for the ceiling). This boundary condition is different from the experimental one where the test section had a floor but no lateral sides or ceiling. The consequence of this boundary condition is that the flow across the lateral sides and the ceiling is permitted

in the experiment but not in the simulation resulting in different 'effective' blocking of the cross section. This will probably have some influence on the aerodynamic forces. No-slip boundary conditions were used on the surface of the body and the instantaneous wall functions based on the log-law (see Krajnović and Davidson (2001) for details) were applied on the channel floor.

Numerical accuracy was established by making three LES on different computational grids containing 3.5, 9.6 and 16.5 millions nodes. The time step was 1×10^{-4}, giving a maximum CFL number of approximately 0.9. The averaging time, tU_∞/H, in the simulations was 38.2 (110,000 time steps).

NUMERICAL METHOD

Equations (1) and (2) are discretized using a 3D finite volume method for solving the incompressible Navier-Stokes equations using a collocated grid arrangement (Davidson and Farhanieh (1995)). Both convective and viscous plus subgrid fluxes are approximated by central differences of second-order accuracy. The time integration is done using the Crank-Nicolson second-order scheme. Although no explicit dissipation is added to prevent odd-even decoupling, an implicit dissipation is present. This is done by adding the difference between the pressure gradient at the face and the node. It can be shown that this term is proportional to the third derivative of pressure, i.e. $\partial^3 p / \partial x_i^3$. This term corresponds to Rhie-Chow dissipation (Rhie and Chow (1983)). The SIMPLEC algorithm is used for the pressure-velocity coupling. The code is parallelized using block decomposition and the PVM and MPI message passing systems (Nilsson and Davidson (1998)).

RESULTS

Although we have collected large amount of results we can present only small fraction in this paper due to space limitations. We chose to present comparison of our LES results and the experimental data for the flow around the rear part of the body. An accurate prediction of time-averaged flow above the slanted surface implies an accurate prediction of the corresponding instantaneous flow. Thus we describe the time instantaneous flow.

COMPARISON OF THE LES RESULTS WITH THE EXPERIMENTAL DATA

This section presents comparison of our LES results with the experimental data of Lienhart and Becker (2003). Although, we have made comparison of all the profiles available in the data files provided from this experimental work, there is no place in this paper to present all the results. Thus we have chosen to present only profiles in the center plane $y = 0$ that were used for comparison in previous CFD studies (Manceau and Bonnet (2000)).

Velocity and Reynolds stresses were measured using a two-component laser-Doppler anemometer (LDA). As we compare LES and experimental profiles we should keep in mind that the experimental data comes from several *different* experimental runs. As we will show later, we have found some discrepancies between our LES profiles and experimental data for some positions which came from one data set and no discrepancies for other positions which were almost identical to the former ones but the experimental data came from another set of experiments. We shall discuss these differences in the following text.

Comparison of the velocity profiles and Reynolds stresses in the plane $y = 0$ are presented in Figs. 3 and 4. Figure 3a) presents streamwise velocity profiles $\langle U \rangle_t$ on the roof and the slanted surface for positions between $x = -0.844H$ and $x = -0.01H$ (from left to right) where the space difference between two profiles is $\Delta x = 0.07H$. The experimental profiles for position $x = -0.774H$ are not available and the LES profiles are presented here only to show the development of the predicted boundary layer at this position. Fine mesh LES (denoted with solid line) overlaps the experimental profiles at all positions except perhaps at the positions on the roof of the body (i.e. $x = -0.844H$ and $-0.705H$). The discrepancies on the roof are probably due to different Reynolds numbers in experiments and our simulations. Although the flow separates on the leading edge of the front end of the body in our simulation (not shown here), the separations region is very thin in both streamwise and wall normal directions. There are no experimental observations of the flow around the front part of the body at the high Reynolds number, but it is reasonable to expect that the separation region becomes thinner as the Reynolds number is increased. Thus the flow on the roof is principally turbulent boundary layer and therefore defined by the viscosity. The Reynolds number in our LES is about four times lower than in the experiments resulting in differences in boundary layer thicknesses. The influence of the Reynolds number is reduced already at the position directly after the upstream sharp edge of the slanted surface (i.e. $x = -0.635H$ in Fig. 3a) and the geometry starts to dictate the downstream flow. The coarse mesh simulation (dashed-dotted curve in the figure) predicts very unrealistic flow with oscillations far above the boundary layer (see the third profile from the left in Fig. 3a)). It is interesting to observe how the change from attached to separated flow downstream of the fourth profile position ($x = -0.635H$) smoothes out these oscillations. Differences between the three LES and the experimental data are smaller in the region of the separation bubble than in the region after the reattachment on the slanted surface (see Fig. 3a)). The coarse mesh simulation predicts too high momentum above the slanted surface in the region after the reattachment. This shows again that the resolution of the near wall structures is much more important in the attached flow region above the lower part of the slant than in the recirculation region above the upper part of the slanted surface.

The $\langle W \rangle_t$ velocities along the slanted surface are for all three

LES in very good agreement with the experimental profiles (see Fig. 3c)). Also here there are some differences between simulations but these appear to be smaller due to smaller magnitude of the $\langle W \rangle_t$ velocities compared to $\langle U \rangle_t$ velocities.

Figures 3b) and d) present $\langle U \rangle_t$ and $\langle W \rangle_t$ velocity profiles in the wake region behind the body for positions x equal with $0.059H$, $0.128H$, $0.132H$, $0.302H$, $0.306H$, $0.479H$, $0.653H$, $0.826H$, H, $1.174H$, $1.521H$, $1.868H$ and $2.215H$ from left to right, respectively. Let us first consider all profiles at all positions except $x = 0.059H$, $0.128H$ and $0.302H$. Although the LES using fine mesh gives almost exact representation of the experimental profiles, all three LES predicted profiles are in very good agreement with the experimental data. Coarse LES have some problems to give accurate representation of the lower recirculating region (see profiles at $x = 0.132H$ and $0.306H$ in 3b) (i.e. the third and the fifth profiles from the left, respectively)) but already the medium simulation capture these regions very well. Let us now return to the remaining three positions (the first, the second and the fourth profiles from the left, i.e. $x = 0.059H$, $0.128H$ and $0.302H$). The experimental data for these profiles are denoted here with circles and comes from a different data set than the one that contains all other profiles in the wake. The experimental profiles for these positions are provided only up to $z = 388mm$ compared to other profiles that goes up to $z = 738mm$. All LES simulations are in relatively poor agreement with experiment in the upper part of the velocities profiles at these positions (see Fig. 3b) and d)). Profiles $x = 0.128H$ (the second profile from the left) and $x = 0.302H$ (the fourth profile from the left) are located at positions that are only $1mm$ from profiles in the first data set, $x = 0.132H$ (the third profile) and $x = 0.306H$ (the fifth profile), respectively. Still the flow in the experimental data changes pretty much between these almost identical positions. Besides, our LES using fine mesh gives exact representation of the experimental profiles from the first data set. Thus we conclude that something is wrong with the experimental data for the second data set (i.e. at the positions $x = 0.059H$, $0.128H$ and $0.302H$).

Figure 4 presents comparison between experimental and LES time-averaged resolved turbulent kinetic energy $\langle k \rangle_t$ and shear stresses $\langle uw \rangle_t$ in the center plane $y = 0$. We shall first concentrate on the flow along the slanted surface in Figs. 4a) and c). The oscillations in the coarse LES of the flow above the roof (the first, the second and the third profiles from the left) found in the velocity field are amplified here (see the third profile from the left in Figs. 4a) and c)). Besides the turbulent kinetic energy is overpredicted in this coarse mesh simulation in the roof flow (see first three profiles from the left in Fig. 4a)). As we move downstream and pass the separation edge (profiles number four, five etc), the oscillations in the coarse LES disappear. All three LES produce slightly lower turbulent kinetic energy than the experiment in the region of recirculating flow (see Fig. 4a)) indicating that the experimental flow is slightly more unsteady than the simulated one. The part of the predicted profiles using
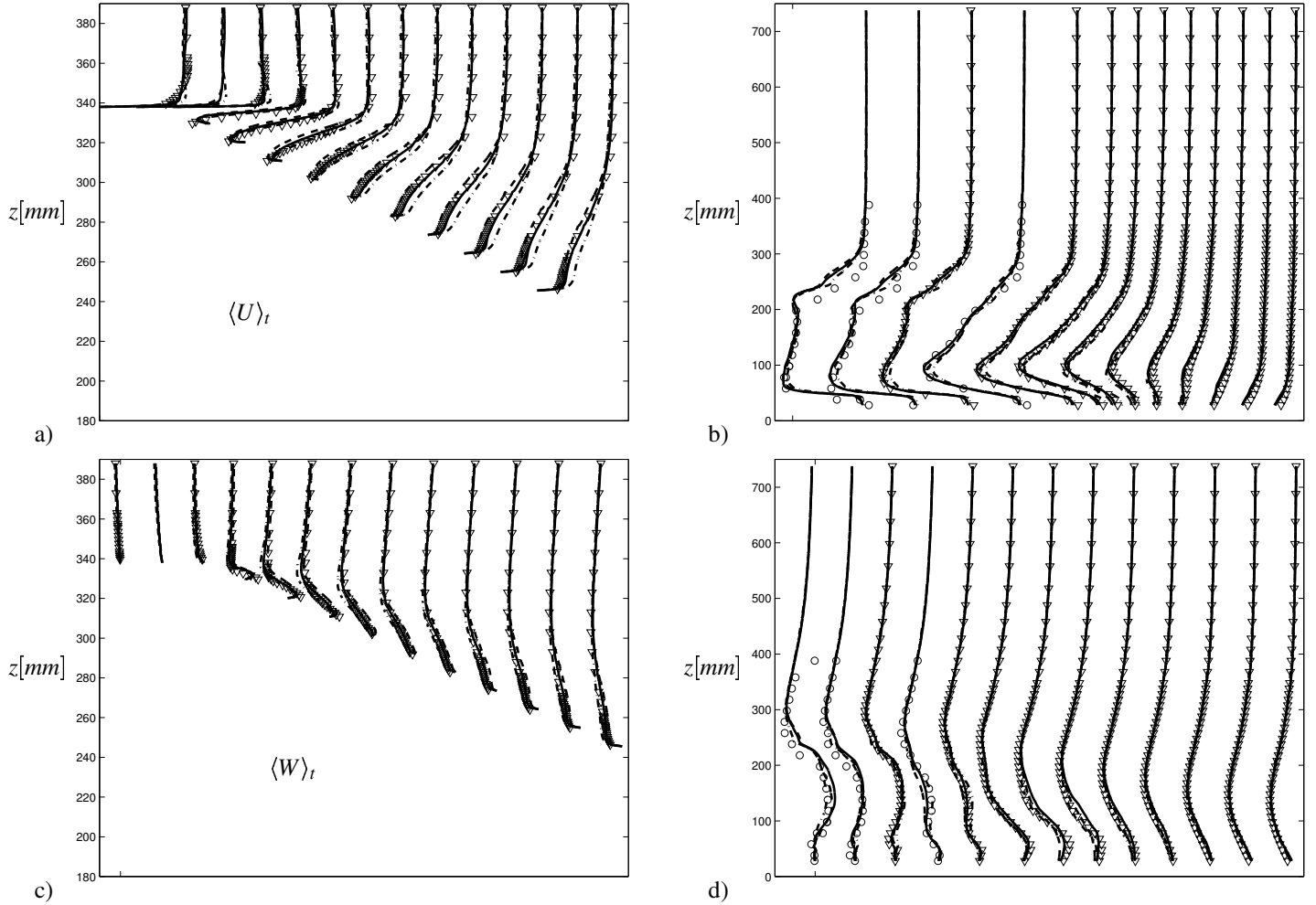
Figure 3. Time-averaged $\langle U \rangle_t$ (Figs. a) and b)) and $\langle W \rangle_t$ (Figs. c) and d)) velocity profiles in the symmetry plane ($y = 0$). Left: slanted surface; right: wake region. Fine grid (solid curve); medium grid (dashed curve); coarse grid (dashed-dotted curve); experiment (symbols).

coarse mesh LES that is above the recirculating region, displays slightly higher resolved turbulent kinetic energy (see the fourth, the fifth and the sixth profiles from the left in Fig. 4a)) similar to that in the upstream flow above the roof. Profiles to the right of the reattachment on the slanted surface are well captured with all LES, although there are some differences in the magnitudes of the profiles between coarse and fine mesh LES on one side and medium mesh on the other side.

The unsteady behavior of the wake flow in our LES is in good agreement with the experimental profiles (see Figs. 4b) and d)). Some differences between the fine mesh LES and the experimental profiles for turbulent kinetic energy are again visible for the positions $x = 0.059H$, $0.128H$ and $0.302H$ (the first, the second and the fourth profiles coming from the different data set compared to the other profiles). The coarse grid LES predicts lower $\langle k \rangle_t$ in the lower part of the profiles at almost all posi-

tions. This is particularly visible in the region around the end of the near-wake separation bubble (the eighth to the tenth profiles from the right in Fig. 4b). The shear stresses $\langle uw \rangle_t$ are under-predicted in the region close to the downstream part of the wake bubble (see Fig. 4d)). We have already seen that the velocity profiles at these positions are in very good agreement with the experimental data in Figs. 3b) and d). Therefore it is difficult to explain these differences between experimental and our LES shear stresses without questioning experimental data in this region.

INSTANTANEOUS FLOW ON THE REAR SLANTED SURFACE This section describes the instantaneous flow structures above the rear slanted surface that are responsible for the time-averaged flow discussed above. As we shall see the flow in this region is very unsteady and complex making it a difficult

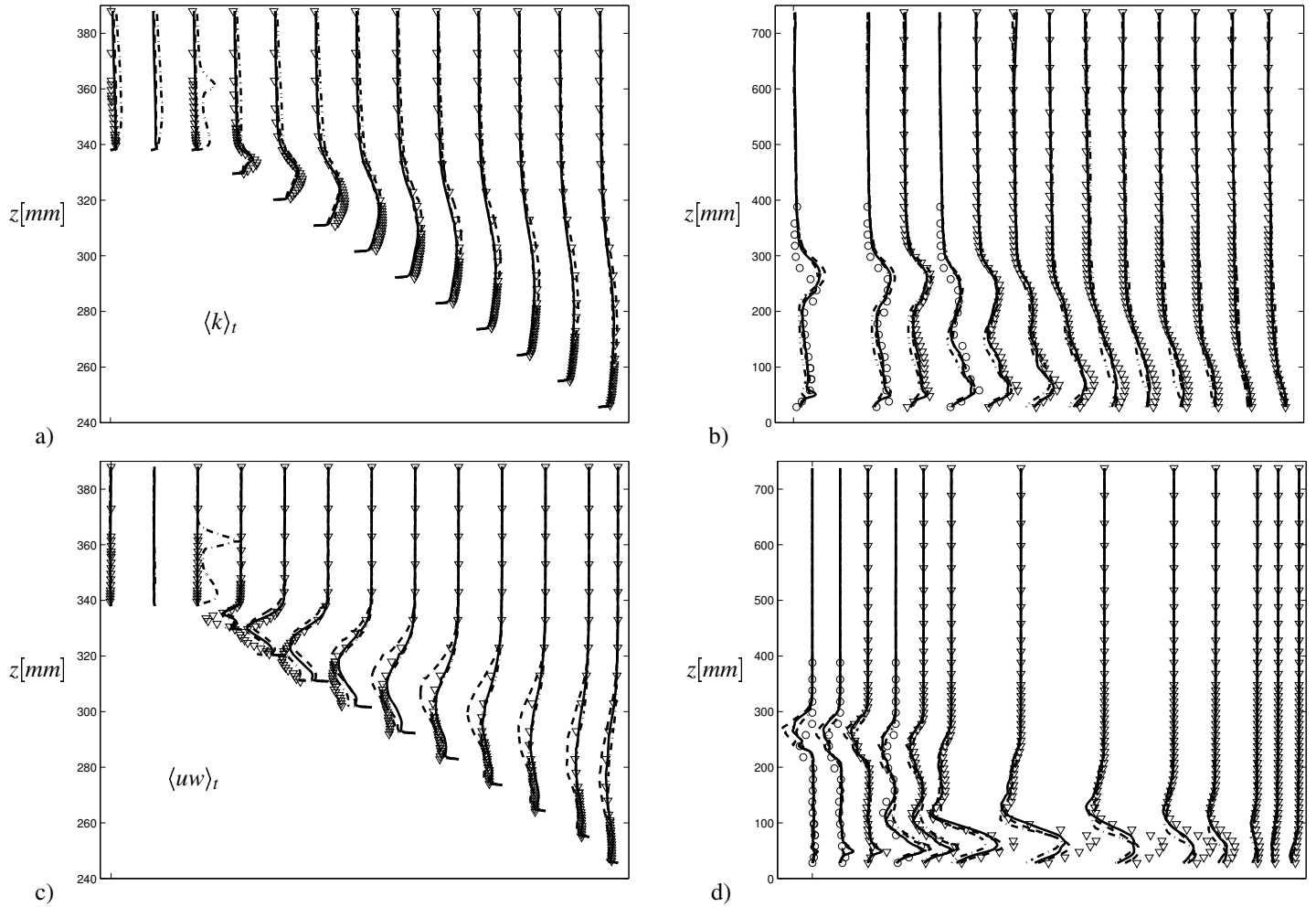7   Copyright © 2004 by ASME

Figure 4. Time-averaged resolved turbulent kinetic energy (Figs. a) and b)) and shear stress (Figs. c) and d)). Left: slanted surface; right: wake region. Fine grid (solid curve); medium grid (dashed curve); coarse grid (dashed-dotted curve); experiment (symbols).

candidate for RANS modeling. The fluid separates at the sharp edge between the roof surface and the slanted rear surface (see Fig. 5). Coherent structures that extend in the spanwise direction are formed as a result of this separation. The axes of these structures are parallel with the edge of separation along the middle part of the edge between the roof and the slanted surface. Those vortices that are born close to the corners of the slanted surface are tilted so that they travel toward the center of the slanted surface. When the spanwise vortices are convected downstream they merge with each other forming slightly larger vortices such as λ_1 in Fig. 5a). Next step in their development is to merge with each other and become bigger such as λ_1 in Fig. 5b) before their tip is lifted from the surface and form hairpin like vortices (see λ_1 in Fig.5c)). Their lifespan as hairpin vortices with both legs on the slanted surface (such as λ_2 in Fig.5a)) is short. One of their legs separates from the surface or is just being broken such as

in λ_2 in Fig. 5b). Finally close to the re-attachment around the half length of the slanted surface the other leg of the vortex is destroyed (see λ_2 in Fig. 5c)) with only small partition continuing downstream and possibly entering the wake region. Vortices traveling downstream are colored with white and those traveling upstream are colored with black. As we can see the recirculation region contains mainly the vortices that travel downstream. They are much stronger than the black-colored vortices close to the surface which are traveling upstream.

The flow coming from the lateral side up over the slant lateral edge separates with high velocity resulting in pressure deficit along the slant edge on the slanted surface side. The fluid roles over the slanted surface from the lateral side to the slanted surface. This takes place on two levels. One thin cone like vortex T_{r1} is formed close to the slant edge with a larger vortex T_{r3} around it (see Fig. 6). These vortices remind of a gearwheel mechanism
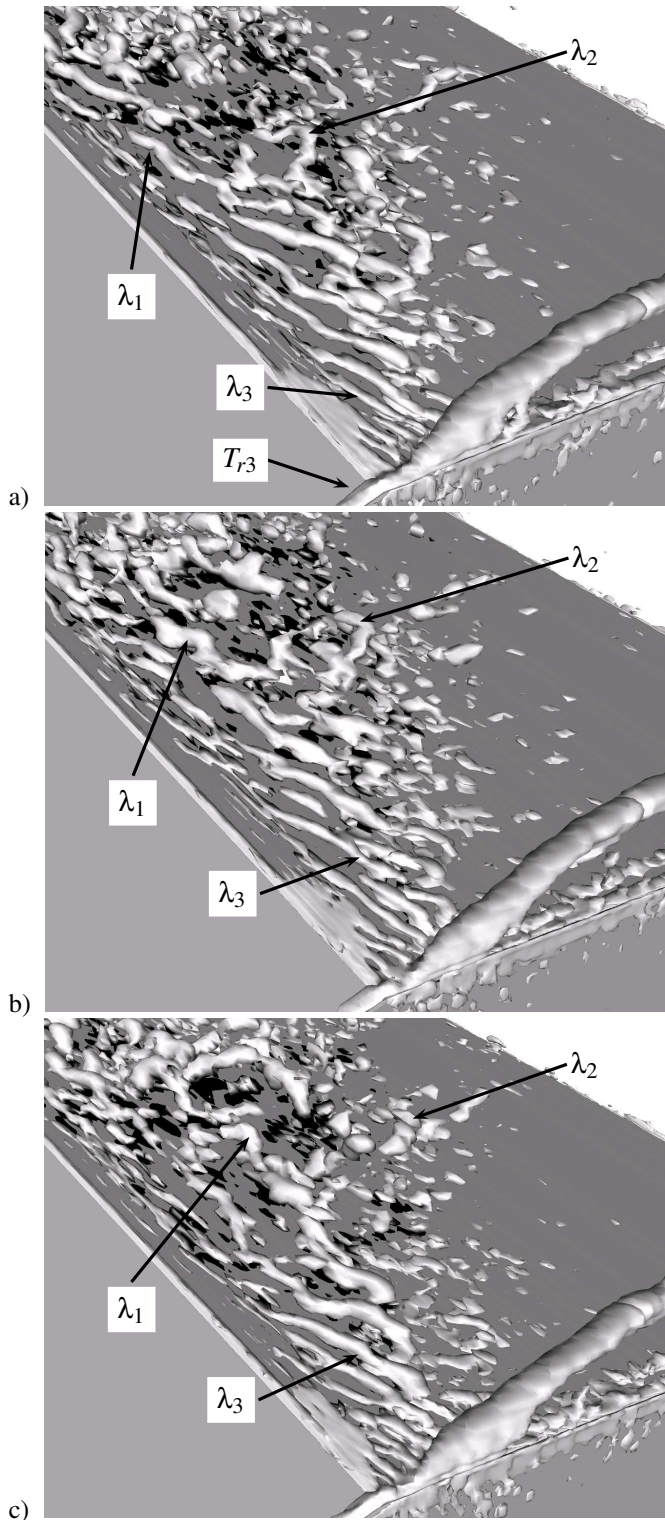
8

Figure 5. The isosurface of the instantaneous second invariant of the velocity gradient, $Q = 6500$. The time difference between two pictures is $tU_\infty/H = 0.055$. Flow is from left to right and the view is from the later side of the body. Vortices are colored by the streamwise velocity. The white vortices are traveling downstream and the black vortices are traveling upstream.

although they are not actually driving each other. The mantle of the vortex T_{r3} (gearwheel number three) that starts as the shear layer on the slanted edge follows the conical path and ends on the slanted surface before it reaches the slanted edge. When its mantle leaves the surface again to continue counter clockwise rotation, it draws the neighboring fluid particles in the upward direction. On the other side the vortex T_{r1} (gearwheel number one) re-attaches on the slanted surface drawing its neighboring fluid particles down toward the surface. These two mechanisms produces the third cone-like vortex T_{r2} (gearwheel number two) with clockwise direction of rotation (see Fig. 6). Only two of these vortices (i.e. T_{r2} and T_{r3}) were observed in previous studies by Ahmed *et al* (1984) and Spohn and Gilleron (2002).

This motion of the fluid from the lateral side to the slanted surface influences partly the upstream flow so that the trailing vortices can be observed upstream of the separation edge between the roof and the slanted surface of the body (see Fig. 5). Here we say 'partly' because some coherent structures are induced already at the front of the lateral edge of the body and convected downstream (not shown here). Similar structures were observed in Spohn and Gillieron (2002) where the motion of fluid from the lateral side to the roof was observed at position $0.25H$ upstream the separation edge.

Let us now return to the spanwise vortices close to the upper corners of the slanted surface (such as λ_3 in Fig. 5). As we already mentioned their axes are tilted with respect to the spanwise edge between the roof and the slanted surfaces. This behavior is caused by the cone like shape of the vortex T_{r3}. As it propagates downstream it grows in the diameter pushing the λ-vortices away from the slant edge. The resulting orientation of the λ-vortices closest to the T_{r3} is toward the center of the slanted surface.

CONCLUSIONS

Our hypothesis of the partial Reynolds number independence of some vehicle flows was confirmed. Although this was demonstrated only for a body with separations strongly defined by the geometry, this shows that LES has large potential in external vehicle aerodynamics.

Using our LES results we have described highly unsteady turbulent mechanisms above the slanted surface. Large differences in the turbulent length scales and the lengths of the turbulence events were registered in this part of the flow.

ACKNOWLEDGMENTS

9

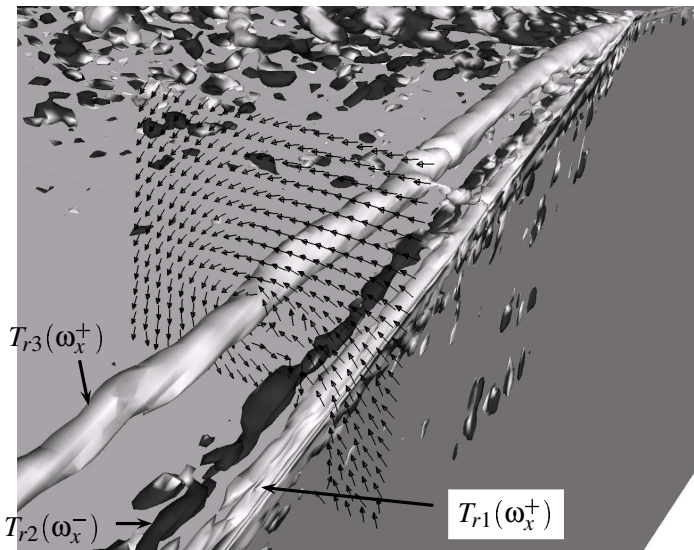Figure 6. The isosurface of the instantaneous second invariant of the velocity gradient, $Q = 6500$. View is from behind of the right slant edge. Note that only core parts of the cone vortices are shown. The cone vortices are colored by the vorticity component in the streamwise direction ω_x. Vortices colored with black and white have clockwise and contour clockwise direction of rotation, respectively.

REFERENCES

Ahmed, S. R., G. Ramm, and G. Faltin (1984). Some salient features of the time averaged ground vehicle wake. SAE Paper 840300.

Cooper, K. R. (1985). The effect of front-edge rounding and rear edge shaping on the aerodynamic drag of bluff vehicles in ground proximity. SAE Paper No. 850288.

Davidson, L. and B. Farhanieh (1995). CALC-BFC: A finite-volume code employing collocated variable arrangement and cartesian velocity components for computation of fluid flow and heat transfer in complex three-dimensional geometries. Report 95/11, Dept. of Thermo and Fluid Dynamics, Chalmers University of Technology, Gothenburg.

Han, T. (1989). Computational analysis of three-dimensional turbulent flow around a bluff body in ground proximity. *AIAA Journal 27*(9), 1213–1219.

Krajnović, S. (2002). *Large Eddy Simulations for Computing the Flow Around Vehicles*. Ph. D. thesis, Dept. of Thermo and Fluid Dynamics, Chalmers University of Technology, Gothenburg.

Krajnović, S. and L. Davidson (2001). Large eddy simulation of the flow around a ground vehicle body. In *SAE 2001 World Congress*, SAE Paper 2001-01-0702, Detroit, Michigan, USA.

Krajnović, S. and L. Davidson (2002). Large eddy simulation of the flow around a bluff body. *AIAA Journal 40*(5), 927–936.

Krajnović, S. and L. Davidson (2003). Numerical Study of the Flow Around the Bus-Shaped Body. *ASME: Journal of Fluids Engineering 125*, 500–509.

Lienhart, H. and S. Becker (2003). Flow and turbulente structure in the wake of a simplified car model. SAE Paper 2003-01-0656.

Manceau, R. and J.-P. Bonnet (2000). 10th joint ERCOFTAC (SIG-15)/IAHR/QNET-CFD Workshop on Refined Turbulence Modelling. Poitiers.

Nilsson, H. and L. Davidson (1998). CALC-PVM: A parallel SIMPLEC multiblock solver for turbulent flow in complex domains. Internal report 98/12, Department of Thermo and Fluid Dynamics, Chalmers University of Technology, Gothenburg.

Rhie, C. and W. Chow (1983). Numerical study of the turbulent flow past an airfoil with trailing edge separation. *AIAA Journal 21*(11), 1525–1532.

Smagorinsky, J. (1963). General circulation experiments with the primitive equations. *Monthly Weather Review 91*(3), 99–165.

Spohn, A. and P. Gillieron (2002). Flow separations generated by a simplified geometry of an automotive vehicle. In *IUTAM Symposium: Unsteady Separated Flows*, April 8-12, Toulouse, France.